Journal of Power Sources 196 (2011) 1639–1644

Contents lists available at ScienceDirect

Journal of Power Sources

journal homepage: www.elsevier.com/locate/jpowsour

Electrospraying tuned photoanode structures for dye-sensitized solar cells with enhanced energy conversion efficiency

Xiaodong Li, Yongzhe Zhang, Zhenxing Zhang, Jinyuan Zhou, Jie Song, Bingan Lu, Erqing Xie*, Wei Lan

School of Physical Science and Technology, Lanzhou University, Lanzhou 730000, Gansu, People's Republic of China

ARTICLE INFO

Article history:
Received 10 May 2010
Received in revised form 6 September 2010
Accepted 8 September 2010
Available online 17 September 2010

Keywords:
Dye-sensitized solar cells
Titanium dioxide
Electrospray coating
Spraying distance

ABSTRACT

Nanocrystalline TiO_2 electrodes have been fabricated using commercially available powers (P25) by electrospray coating (ESC) method. The structures and morphologies of the film, which ultimately influence the cell performance, can be controlled by changing the distance between the capillary nozzle and the FTO substrate (spraying distance). A possible mechanism of the evolution of the structures and morphologies has been discussed in detail. The optimized spraying distance for the maximum short-circuit photocurrent density of the cells is 6 cm, while accompanying with the lowest fill factor. The improvement of short-circuit photocurrent density can be mainly ascribed to the better ion-diffusion path, which is caused by presence of the electrolyte "relay stations" in the film. The low fill factor may be attributed to the increase of the resistance at FTO/TiO_2 interface, which may be caused by the secondary spheres in the film. In addition, enhanced energy conversion efficiencies have been observed by using a double-layer structure, which consists of a doctor-bladed 7-μm bottom layer and an electrospray coated 10-μm top layer.

1. Introduction

Dye-sensitized solar cells (DSCs) have attracted extensive interest due to its easy, low-cost, and environment-friendly preparation process [1–3]. As well known, DSCs can convert visible light energy to electrical energy by a charge separation process in sensitizer dyes adsorbed on the photoanode which is usually made from wide band gap semiconductors. The photoanode is a key component in DSCs, because it can act as a scaffold for the dyes and a transfer media for photogenerated electrons to the F-doped tin oxide (FTO) layer. Up till now, various techniques such as screen printing [4–6], doctor blade [7,8], electrophoretic deposition [9,10], and spray pyrolysis deposition (SPD) [11–13] have been developed to fabricate the photoanode for DSCs. However, each of the methods has its disadvantages [14,15], such as limited control over the morphology and microstructure, time consuming and energy cost, creating closed pores instead of open ones. Therefore, with the purpose of improving the performance of DSCs and making the fabrication process suitable for industrial production, it is urgent and important to develop an easy, low-cost, and stable technique to prepare the photoanode for DSCs.

Electrospray coating is a method of liquid atomization by electrical forces [16]. As a deposition technique, ESC possesses many advantages, large-area preparation, various geometries of the substrate, high deposition rate, and so on. Moreover, electrospraying devices can work under the atmospheric ambience, which make it an energy saving and low-cost technology. Therefore, ESC might be a promising method for the preparation of photoanode for the industrial manufacture of DSCs. However, this excellent technique has not been sufficiently studied in the field of DSCs [15,17].

On the other hand, various approaches have been developed to optimize the photoanode structures and morphologies for the purpose of improving the cell performance, such as using hierarchically structured film consisting of secondary colloidal spheres to improve light harvesting [18,19], coupling carbon nanotubes to the electrode can promote the electron transfer through it [20–22], and fabricating better ion-diffusion path in the electrode [14,23]. With regard to the hierarchically structured film, there are some irreconcilable factors, such as the small contact area among the spheres would make it difficult to transfer the electrons to the neighboring spheres. Therefore, in this work, hierarchically structured films were fabricated by using ESC technique by simply adjusting the spraying distance. Results show good connection between the spheres within the films at a suitable spraying distance, and enhanced energy conversion efficiencies of the DSCs have been observed.

2. Experiment

2.1. Preparation of TiO_2 paste

TiO_2 paste was prepared by a two-step process. First, 0.09 g of polyvinyl pyrrolidone (PVP, Sigma–Aldrich, $M_w \approx 1{,}300{,}000$) was

* Corresponding author. Fax: +86 931 8913554.
E-mail addresses: lixd04@163.com (X. Li), xieeq@lzu.edu.cn (E. Xie).

0378-7753/$ – see front matter © 2010 Elsevier B.V. All rights reserved.
doi:10.1016/j.jpowsour.2010.09.017

Table 1
Summary of the applied voltage that kept the electrospraying working stably at cone-jet mode and the optimal photoanode thickness (d_{optim}) at which the maximum conversion efficiency was obtained for cells fabricated under different spraying distances.

	Spraying distance (cm)				
	2.5	5	6	7	9
Applied voltage (kV)	4.5	6.5	7.2	7.8	8.2
d_{optim} (μm)	13	15	18	20	20

dissolved in 1.8 mL of ethanol by vigorous magnetic stirring for 20 min. Second, 1.2 g of TiO_2 powder (P25, Degussa) was grinded under acetic acid in an agate mortar for 30 min. In this case, about 1 mL of acetic acid was added drop by drop during the grinding process which can prohibit the TiO_2 particles from the aggregation [4]. Then 4 mL of deionized water was added into the agate mortar drop by drop during grinding, and the suspension was again grinded for 20 min. Subsequently, the suspension was added into PVP ethanol solution drop by drop under strong stirring. After stirring for 15 min, TiO_2 paste was obtained.

2.2. Fabrication of TiO_2 electrodes

TiO_2 electrodes were fabricated by ESC technique, which has been described in our previous work [15]. The spraying distance varied from 2.5 cm to 9 cm, and the voltage applied between the capillary nozzle and the metallic collectors was adjusted to keep electrospraying working at cone-jet mode. The applied voltages were listed in Table 1. Before the electrospraying process, FTO glass (2.2 mm in thickness, >90% transmittance, 14 Ω/□, Nippon, Japan) were pretreated using a 40 mM $TiCl_4$ aqueous solution at 70 °C for

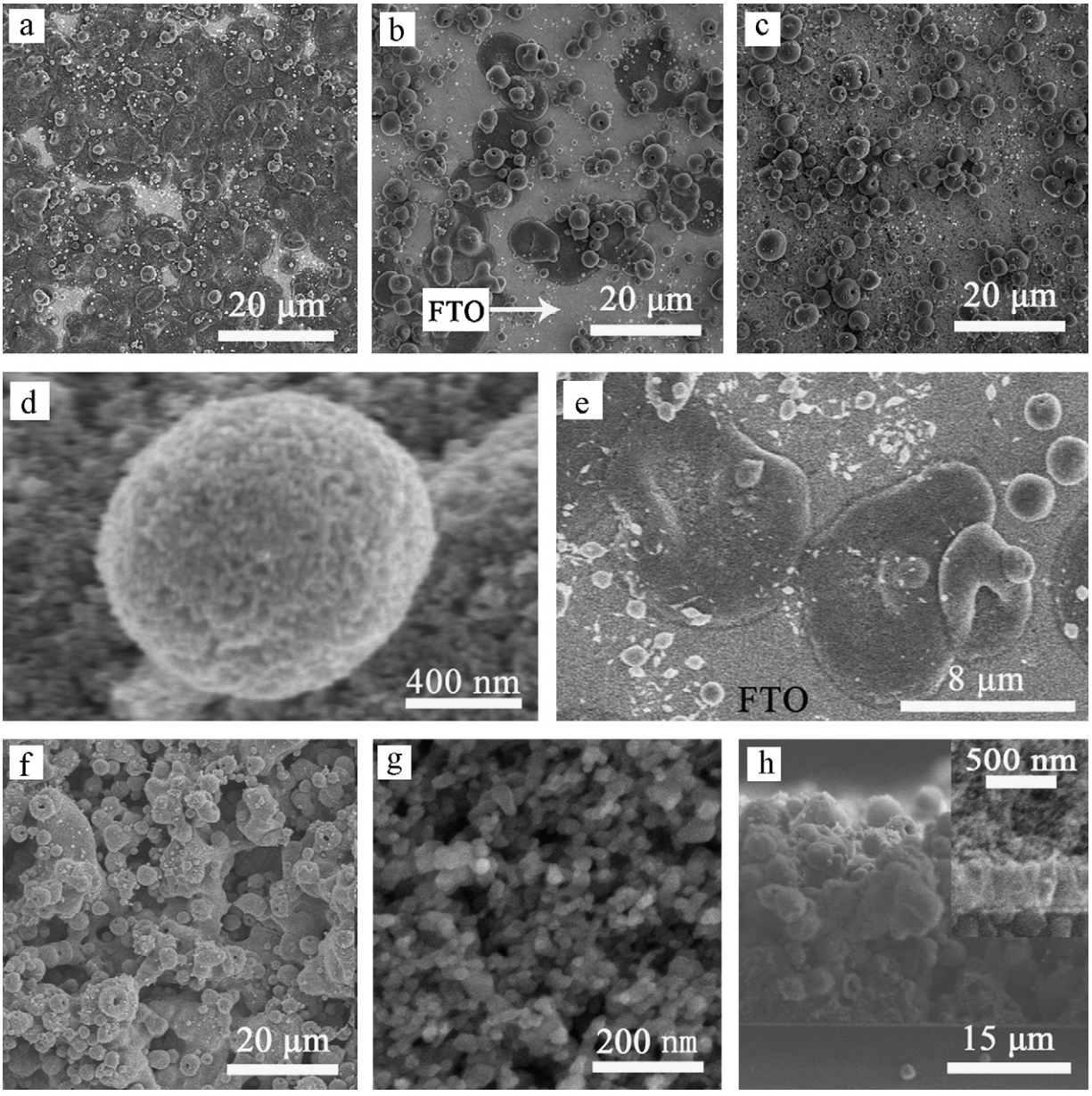

Fig. 1. FESEM images of TiO_2 electrodes. As-sprayed samples prepared under spraying distances of 2.5 cm (a), 6 cm (b) and 9 cm (c). Details of the secondary spheres (d) and flat droplets (e). Morphologies (f and g) and cross-section (h) of a nanocrystalline TiO_2 electrode prepared under a spraying distance of 6 cm and sintered at 450 °C for 1 h.

30 min, and then successively washed with deionized water and ethanol for several times. To reduce the charge accumulation on the surface of the substrate during electrospraying, the conducting layers of FTO glass were connected to the collectors.

2.3. Assembling of DSCs

Before the assembling of DSCs, all TiO_2 electrodes were sintered at 450 °C for 1 h. At 80 °C in the cooling, the sintered TiO_2 electrodes were immersed into a 0.3 mM solution of N-719 dye in a mixture of tert-butyl alcohol and acetonitrile (volume ratio of 1:1) and kept in the dark at room temperature for 12 h to complete the adsorption of the dye. Then the dye-adsorbed TiO_2 electrodes were rinsed with ethanol for 1 h to remove the physisorbed dye molecules. The platinized electrodes were prepared by spin coating a 4.5 mM isopropanol solution of H_2PtCl_6, and then heated at 400 °C for 20 min. The platinized counter electrode and dye-adsorbed TiO_2 electrode were assembled into a sandwich-type cell. Finally, a drop of electrolyte, a solution of 0.1 M LiI, 0.6 M 1,2-dimethyl-3-propylimidazorium iodide, 0.05 M I_2 and 0.5 M 4-tert-butylpyridine in acetonitrile was injected into the space between the two electrodes. The cell area was 0.27 cm^{-2}.

2.4. Characterizations of TiO_2 electrode and cell performance measurements

The thicknesses of TiO_2 electrode were obtained by using a surface profile measurement system (Veeco, Dektak8 ADP-8), and their morphologies and absorption behavior were studied by field emission scanning electron microscopy (FESEM, Hitachi, S-4800) and UV-VIS-NIR spectrophotometer (Shimadzu, UV-3600), respectively. Performance of the cells was characterized by external resistance loads employing a solar simulator (85 mW cm^{-2}).

3. Results and discussion

3.1. Structures and morphologies of the electrospray coated TiO_2 films

3.1.1. Tuning of the film structures and morphologies by varying spraying distance

The typical SEM images of the samples fabricated under different spraying distances (2.5 cm, 6 cm and 9 cm) are shown in Fig. 1(a)–(c). In order to study the effect of the spraying distance on the structures of the samples, the preparation times of the samples were so short that the surface of the substrate had not been completely covered. It can be seen that the samples consist of many secondary spheres and flat droplets (Fig. 1(a) and (b)), and the number and size of the secondary spheres increase with the increase of spraying distance (Fig. 1(a)–(c)). The secondary spheres and the flat droplets are made up of primary TiO_2 nanoparticles (P25) (Fig. 1(d) and (e)). At a spraying distance of 9 cm, no flat droplet can be observed (Fig. 1(c)).

Tuning of the structures and morphologies of the film by changing the spraying distance is shown in Fig. 2. The droplets produced at the end of the jet possess a wide size distribution in this work. In the ESC process, under certain spraying distance, the droplets with sizes less than a cut-off value, at which the solvent in the droplets vaporize entirely just above the substrate, change into dry secondary spheres; while the droplets with sizes larger than the cut-off value are only partially dried due to the smaller specific surface area than the droplets with sizes less than a cut-off value. The partially dried droplets with a variable shape change into flat droplets when they impact the FTO substrate which can result in good connection between the secondary spheres (Fig. 2), and thus the whole film. As the spraying distance increases, the cut-off value

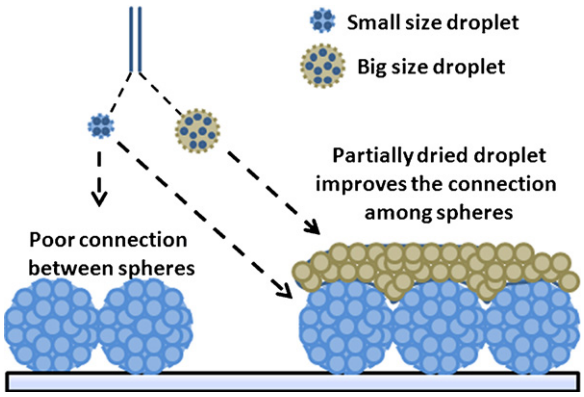

Fig. 2. Diagram showing improvement of the connection among spherical structures.

increases, and at a spraying distance of 9 cm, even the droplets with biggest size can change into secondary spheres as shown in Fig. 1(c).

3.1.2. Morphologies and cross-section of the TiO_2 electrode

Fig. 1(f)–(h) shows the morphologies and cross-section of TiO_2 electrode prepared under a spraying distance of 6 cm and sintered at 450 °C for 1 h. Fig. 1(f) shows that the film is made up of spheres with diameter about several micrometers, and the good connection between these spheres can be attributed to the presence of the flat droplets. The films containing too many aggregates usually shrinkage largely while sintering, resulting in the peering-off from the substrate [4]. That is to say, the number of the aggregates in the films should be controlled to a minimum value. From Fig. 1(g), it can be found that the film consists of homogeneously dispersed nanoparticles and few aggregates can be observed. Furthermore, the films fabricated under a spraying distance of 6 cm have a good adhesion with the FTO substrate, even the thickness of the films is high up to 22 μm (Fig. 1(h), inset).

We found that it is difficult to fabricate the films with thickness larger than 13 μm by using the doctor blade method. This may be due to the shrinkage of the film during the solvent evaporation process. The films prepared by ESC are mainly composed of the droplets that evolved from the atomization of the precursor solution or colloidal suspension. Thus, it may rank among the "bottom-up" technique [16]. The droplets will vaporize partially, even entirely during flying to the substrate. Thus, this technique may relieve the stress in the films and depress the shrinkage to a certain degree.

3.2. The effect of spraying distance on DSCs photovoltaic-characteristics

Photovoltaic-characteristics depending on the spraying distances are shown in Fig. 3. As the spraying distance increases, the short-circuit photocurrent density (J_{sc}, Fig. 3(a)) rises up to a maximum value of 11.60 mA cm^{-2} at 6 cm and then decreases sharply. The open-circuit voltage (V_{oc}, Fig. 3(b)) increases with the spraying distance increasing. It can be seen that the fill factor (FF, Fig. 3(c)) decreases to a minimum value of 0.56 at a spraying distance of 6 cm. The variation of J_{sc}, V_{oc} and FF reflects on the variation trend of the total energy conversion efficiency (η), which has a peak at a spraying distance of 6 cm (Fig. 3(d)). It is necessary to point out that the film thicknesses needed to obtain the maximum conversion efficiency of the cells are variable for different spraying distances. The optimal thicknesses of the samples (d_{optim}) under different spraying distances are listed in Table 1.

According to the previous research [17–19], two reasons may be responsible for the increase of J_{sc} when the spraying distances

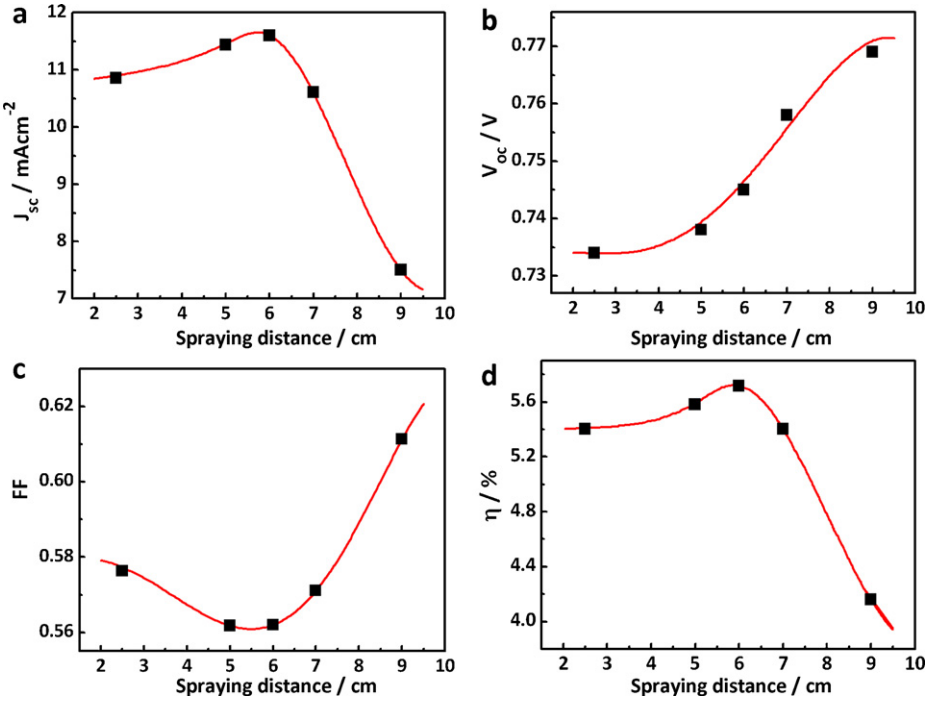

Fig. 3. Spraying distance dependent photovoltaic-characteristics relationships: J_{sc} (a), V_{oc} (b), FF (c) and conversion efficiency (η) (d), each point is an average of three samples.

is less than 6 cm. One is related to the light absorption behavior enhanced by the secondary spheres in the films. The spheres with diameter larger than 100 nm can enhance the photon absorption by way of light scattering [18]. According to the scattering theory, effective Mie scattering happen to the particles with size in the range of light wavelengths [24]. However, the size and the size distribution (the most probable diameter of the spheres is larger than 1 μm) in this work is not an optimized result. Thus, the contribution of light scattering to the increase of J_{sc} is little, which can be demonstrated by the small difference of the absorption behavior between the films prepared under spraying distances of 6 cm and 2.5 cm (Fig. 4).

The other factor is the diffusion limitation of the ions in the electrolyte. Several research groups have investigated the diffusion limitation of the ions in the electrolyte by measuring the current–voltage characteristics of simple Pt-electrolyte-Pt sandwich devices with a porous TiO_2 layer sintered directly onto one of the Pt electrodes [17,25–26]. Such a device structure allows for the catalyzed reaction of the I^-/I^-_3 system at both electrodes even with very low voltages applied. In contrast to the dark current measurement (in dark) of DSCs, there is an onset point over 0.4 V from which the TiO_2 film becomes conductive and the current density increases rapidly [27]. Therefore, for such a device, ion transport mainly proceeds from Pt electrode to Pt electrode, namely, electron injections from the TiO_2 surface were negligible [17,26]. This enables us to study the diffusion properties of the ions through nanocrystalline TiO_2 films fabricated under different spraying distances.

As shown in Fig. 5, the limiting current density increases with the spraying distance increasing, regardless of the voltage potential polarity. This indicates that the films prepared under larger spraying distance show better ionic paths due to the presence of the secondary spheres. A schematic diagram can be drawn to illustrate the differences between the TiO_2 films with compact packing of nanoparticles (under spraying distance of less than 2.5 cm) and the ones with poor packing of spherical structures (fabricated under large spraying distance), as shown in Fig. 6. The former only possesses path A, which stands for the random paths consisting of the tiny voids among the nanoparticles, while the latter shows an addi-

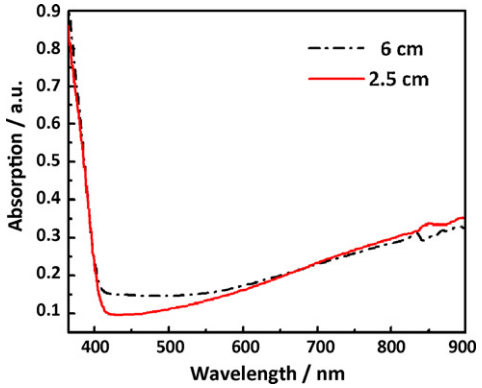

Fig. 4. Plot of the absorption behavior of TiO_2 films on FTO prepared under the spraying distance of 6 cm and 2.5 cm.

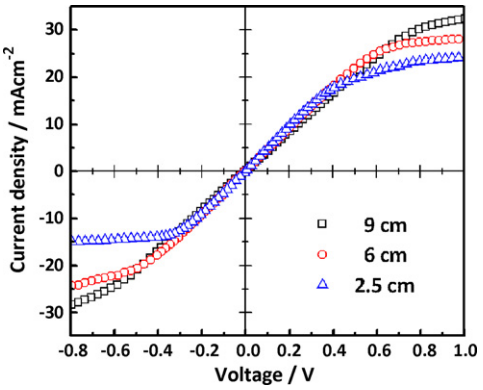

Fig. 5. Current–voltage characteristics of the simple Pt/TiO_2-electrolyte-Pt sandwich devices with the nanocrystalline TiO_2 films prepared under various spraying distances (for clarity, only data for spraying distance 2.5 cm, 6 cm and 9 cm are shown). The voltage polarity refers to the Pt/TiO_2 electrode.

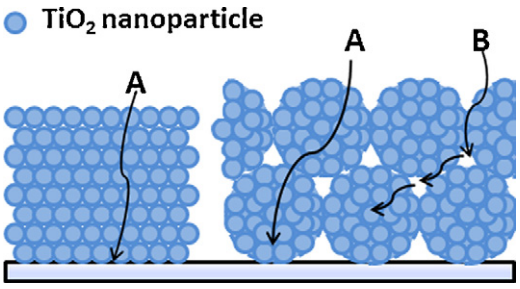

Fig. 6. Diagram showing differences of the ion diffusion paths between the TiO_2 films with compact packing of nanoparticles (left) and the ones with poor packing of the spherical structure (right).

tional path B, which represents the path via the interspaces among the spheres. The interspaces among the spheres can act as "relay stations" for electrolyte diffusion, which can help the ions transport through the film more efficient.

The films obtained under large spraying distance show a loose packing, leading to the increase of void volume in the samples and decrease of the film density (Fig. 7). The increase of void volume is beneficial to the ion transport, which may be responsible for the increase of J_{sc}. However, when the spraying distance is larger than 6 cm, increasing spraying distance will lead to the sharp decease of TiO_2 nanoparticle loading (Fig. 7), which can result in the decrease of J_{sc}.

Moreover, the decrease of nanoparticle loading results in the reduction of the charge recombination sites, and thus the dark current, which is beneficial to the V_{oc} (Fig. 3b). As evidence, we measured the dark currents (in dark) for cells fabricated at different spraying distances and found that the current density at a certain negative bias decreased with increasing spraying distance (not shown). To a certain extent, increase of the V_{oc} with increasing spraying distance is equivalent to increasing the V_{oc} by decreasing the film thickness. The thick films provide additional charge-recombination sites, leading to the increase of the dark current, which is detrimental to V_{oc} [28,29].

The secondary spheres collected on the surface of FTO layer reduce the contact area between the films and the substrate, leading to a larger resistance at FTO/TiO_2 interface, which can affect fill factor [30]. Therefore, the low FF at spraying distance of 6 cm can be ascribed to the increase of the proportion of the secondary spheres to flat droplets. Moreover, when the spraying distance is larger than 6 cm, the increase of FF can benefit from the reduction of dark current due to the sharply decrease of TiO_2 nanoparticle loading (Fig. 7). Of course, in this case, when the spraying distance is larger than 6 cm the samples possess larger internal resistance

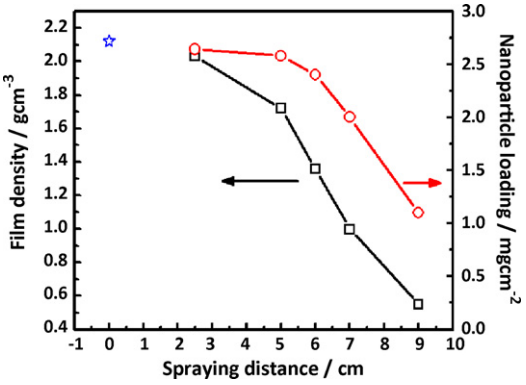

Fig. 7. Film density and nanoparticle loading of the TiO_2 electrodes as function of the spraying distance. The point plotted at spraying distance of 0 cm is the film density of doctor-bladed TiO_2 electrodes.

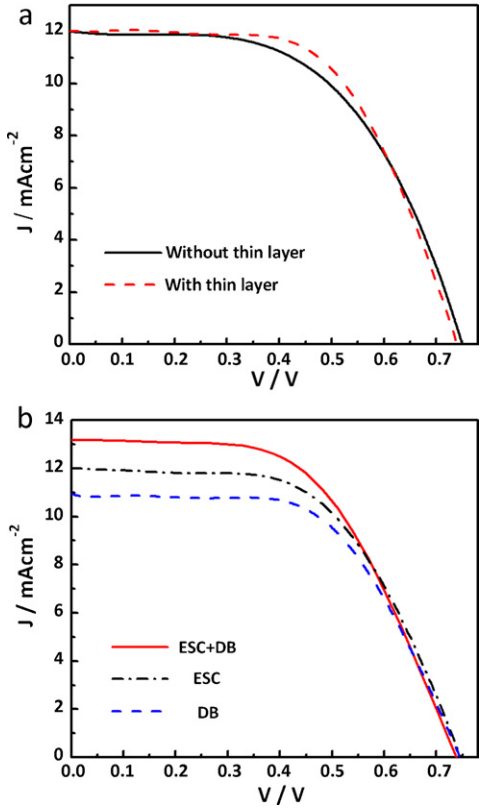

Fig. 8. *I–V* curves for DSCs (a) with and without a doctor-bladed thin layer at the bottom of the electrospray coated 17-μm thick film under the spraying distance of 6 cm, and (b) fabricated by ESC method, doctor blade method and combination of the above two methods.

at FTO/TiO_2 interface than the samples fabricated under a spraying distance less than 6 cm, whereas the sharply reduction of dark current due to the decrease of TiO_2 nanoparticle loading may change into dominant cause.To assess the validity of the above analysis of the cause of the low FF, a thin nanocrystalline TiO_2 layer (~1 μm) was fabricated on the FTO substrate by doctor blade method using the TiO_2 suspension without PVP prior to the fabrication of a 17 μm thick TiO_2 layer by using ESC technique under spraying distance of 6 cm. *I–V* behaviors shown in Fig. 8(a) indicate that the cells with thin nanocrystalline TiO_2 layer show an enhanced fill factor from 0.56 to 0.59. It is necessary to point out that the short-circuit photocurrent density of the two *I–V* curves in Fig. 8(a) nearly has the same values and has been normalized to the same value for the purpose of clearly displaying the difference between them. The increase of the FF demonstrates that the resistance at FTO/TiO_2 could affect the fill factor of the cell. In addition, a simple method to improve the fill factor has been verified.

3.3. The double-layer cell

Compared with the electrodes fabricated by doctor blade method, the electrodes fabricated by ESC under the spraying distance of 6 cm show an evident drawback that the film density is very low (Fig. 7). Thus, we combined these two methods to fabricate the cells with a double-layer structure. First, a 7-μm-thick layer was fabricated by doctor blade method, and then a 10-μm-thick layer was prepared by ESC on it. Both layers were fabricated by using the same TiO_2 paste. As shown in Fig. 8(b), the best energy conversion efficiency for the cells fabricated by doctor blade method and ESC method is 5.60% and 5.97%, respectively, while the energy conversion efficiency for the double-layer cell has been improved up to

6.28%. This may be due to the combination of the respective advantages of the two methods: the bottom layer fabricated by doctor blade method show a larger density of TiO_2 particles and more dye molecules can be attached to it; the top layer let the ions in the electrolyte diffuse to the bottom layer easier than a single 17 μm thick film by doctor blade was used.

4. Conclusion

TiO_2 nanocrystalline electrodes were successfully fabricated by ESC method using a P25 based paste which is suitable for ESC technique. By taking advantage of the differences in solvent evaporation rate of the droplets with different sizes, the structures and morphologies of the film can be tuned by varying the spraying distance. The interspaces among the spheres which act as "relay stations" for electrolyte transport are mainly responsible for the enhancement of the photocurrent density, and thus the total energy conversion efficiency. However, the fill factor of the cells with maximum short-circuit photocurrent density is the lowest due to the smaller contact area resulting from the increase of the proportion of secondary spheres to flat droplets. The maximum energy conversion efficiency obtained by doctor blade and ESC is 5.60% and 5.97%, respectively. Combination of the two methods can make an enhanced energy conversion efficiency of 6.28%.

By taking advantage of the differences in solvent evaporation rate of the droplets with different sizes, spherical structures and partially dried droplets can be deposited simultaneously, which would be a practical way to achieve good electron transfer property between neighboring spheres in the hierarchically structured film. The simple way to tune the structures and morphologies of the film can contribute not only to the research of DSCs, but also to various applications related to ESC.

Acknowledgments

This work was financially supported by the Fundamental Research Funds for the Central Universities (No. lzujbky-2010-82), partially by the National Natural Science Foundation of China (No. 50802037) and the Fundamental Research Funds for the Central Universities (No. lzujbky-2009-56).

References

[1] B. O'Regan, M. Grätzel, Nature 353 (1991) 737–740.
[2] B.E. Hardin, E.T. Hoke, P.B. Armstrong, J.H. Yum, P. Comte, T. Torres, J.M.J. Frechet, M.K. Nazeeruddin, M. Grätzel, M.D. McGehee, Nat. Photonics 3 (2009) 406–411.
[3] H.J. Snaith, Adv. Funct. Mater. 20 (2010) 13–19.
[4] S. Ito, P. Chen, P. Comte, M.K. Nazeeruddin, P. Liska, P. Péchy, M. Gräzel, Prog. Photovoltaics: Res. Appl. 15 (2007) 603–612.
[5] T. Ma, T. Kida, M. Akiyama, K. Inoue, S. Tsunematsu, K. Yao, H. Noma, E. Abe, Electrochem. Commun. 5 (2003) 369–372.
[6] S. Ito, T.N. Murakami, P. Comte, P. Liska, C. Grätzel, M.K. Nazeeruddin, M. Grätzel, Thin Solid Films 516 (2008) 4613–4619.
[7] S. Ito, T. Kitamura, Y. Wada, S. Yanagida, Sol. Energy Mater. Sol. Cells 76 (2003) 3–13.
[8] W. Chen, X. Sun, Q. Cai, D. Weng, H. Li, Electrochem. Commun. 9 (2007) 382–385.
[9] T. Miyasaka, Y. Kijitori, J. Electrochem. Soc. 151 (2004) A1767–A1773.
[10] G.-S. Kim, H.-K. Seo, V.P. Godble, Y.-S. Kim, O.B. Yang, H.-S. Shin, Electrochem. Commun. 8 (2006) 961–966.
[11] M. Okuya, K. Nakade, S. Kaneko, Sol. Energy Mater. Sol. Cells 70 (2002) 425–435.
[12] M. Okuya, K. Nakade, D. Osa, T. Nakano, G.R. Asoka Kumara, S. Kaneko, J. Photochem. Photobiol. A: Chem. 164 (2004) 167–172.
[13] C.H. Chen, F.L. Yuan, J. Schoonman, Eur. J. Solid State Inorg. Chem. 35 (1998) 189–196.
[14] E. Khaleghi, E. Olevsky, M. Meyers, J. Am. Ceram. Soc. 92 (2009) 1487–1491.
[15] Y. Zhang, L. Wu, E. Xie, H. Duan, W. Han, J. Zhao, J. Power Sources 189 (2009) 1256–1263.
[16] A.T.S.A. Jaworek, J. Electrostat. 66 (2008) 197–219.
[17] M. Fujimoto, T. Kado, W. Takashima, K. Kaneto, S. Hayase, J. Electrochem. Soc. 153 (2006) A826–A829.
[18] T.P. Chou, Q. Zhang, G.E. Fryxell, G.Z. Cao, Adv. Mater. 19 (2007) 2588–2592.
[19] Z. Yong-Zhe, W. Li-Hui, L. Yan-Ping, X. Er-Qing, Y. De, C. Jiang-Tao, Chin. Phys. Lett. 26 (2009) 038201.
[20] S.L. Kim, S.R. Jang, R. Vittal, J. Lee, K.J. Kim, J. Appl. Electrochem. 36 (2006) 1433–1439.
[21] T.Y. Lee, P.S. Alegaonkar, J.-B. Yoo, Thin Solid Films 515 (2007) 5131–5135.
[22] S. Pimanpang, W. Maiaugree, W. Jarernboon, S. Maensiri, V. Amornkitbamrung, Synth. Met. 159 (2009) 1996–2000.
[23] Y. Zhao, X.L. Sheng, J. Zhai, L. Jiang, C.H. Yang, Z.W. Sun, Y.F. Li, D.B. Zhu, Chemphyschem 8 (2007) 856–861.
[24] J. Ferber, J. Luther, Sol. Energy Mater. Sol. Cells 54 (1998) 265–275.
[25] N. Papageorgiou, C. Barbe, M. Grätzel, J. Phys. Chem. B 102 (1998) 4156–4164.
[26] M. Dürr, G. Kron, U. Rau, J.H. Werner, A. Yasuda, G. Nelles, J. Chem. Phys. 121 (2004) 11374–11378.
[27] B.A. Gregg, F. Pichot, S. Ferrere, C.L. Fields, J. Phys. Chem. B 105 (2001) 1422–1429.
[28] Z.-S. Wang, H. Kawauchi, T. Kashima, H. Arakawa, Coord. Chem. Rev. 248 (2004) 1381–1389.
[29] S. Ito, S.M. Zakeeruddin, R. Humphry-Baker, P. Liska, R. Charvet, P. Comte, M.K. Nazeeruddin, P. Péchy, M. Takata, H. Miura, S. Uchida, M. Grätzel, Adv. Mater. 18 (2006) 1202–1205.
[30] T. Hoshikawa, M. Yamada, R. Kikuchi, K. Eguchi, J. Electrochem. Soc. 152 (2005) E68–E73.